Available online at www.sciencedirect.com
ScienceDirect
Applied Thermal Engineering 27 (2007) 1722–1727
Applied Thermal Engineering
www.elsevier.com/locate/apthermeng

Measurement and modeling of liquid film thickness evolution in stratified two-phase microchannel flows

Julie E. Steinbrenner *, Carlos H. Hidrovo, Fu-Min Wang, Sebastien Vigneron, Eon Soo Lee, Theresa A. Kramer, Ching-Hsiang Cheng, John K. Eaton, Kenneth E. Goodson

Department of Mechanical Engineering, Stanford University, 440 Escondido Mall, Building 530 Room 224, Stanford, CA 94305, USA

Received 20 January 2006; accepted 27 July 2006
Available online 27 September 2006

Abstract

Polymer electrolyte membrane (PEM) fuel cells incorporating microchannels ($D < 500$ μm) can benefit from improved fuel delivery and convective cooling. However, this requires a better understanding of two-phase microchannel transport phenomena, particularly liquid–gas interactions and liquid clogging in cathode air-delivery channels. This paper develops optical fluorescence imaging of water films in hydrophilic channels with varying air velocity and water injection rate. Micromachined silicon test structures with optical access and distributed water injection simulate the cathode channels of a PEM fuel cell. Film thickness data vary strongly with air velocity and are consistent with stratified flow modeling. This work facilitates the study of regime transitions in two-phase microchannel flows and the effects of flow regimes on heat and mass transfer and axial pressure gradients.

Keywords: Stratified flow; Microchannel; Fluorescent imaging; Two-phase; Liquid film

1. Introduction

The polymer electrolyte membrane (PEM) fuel cell is a promising portable energy conversion device for an emerging sustainable energy economy. Recent efforts to improve the efficiency and power density of PEM fuel cells have led to a reduction in size of the gas delivery channels. While these microscale channels promise performance improvements [1], they also present challenges in terms of water management within the fuel cell and the associated heat transfer and thermal management challenges [2]. Liquid water both enables and impedes the performance of a PEM fuel cell. While necessary in the membrane for proton conduction, liquid water in the gas diffusion layer and channels obstructs the transport of reactants to the catalyst sites [1,3,4]. Therefore, excess water produced at the cathode of the PEM fuel cell must be evacuated quickly. Furthermore, in small channels surface tension dominates and can lead to flooding of the diffusion layer and clogging of the gas channels. Design for optimal performance requires a thorough understanding of the interaction between surface tension, phase change and convective transport in the two-phase flow in the cathode microchannels.

Despite its impact on the performance of PEM fuel cells, there has been relatively little previous work on determining liquid–gas flow regimes and detecting liquid film thicknesses in microchannels. Some liquid imaging work has been performed using gamma densitometry, X-ray tomography, and capacitive sensors [5,6]. However, these measurement techniques do not allow microscale flow regime characterization, which is of particular concern in this application. Therefore, optical techniques providing flow visualization are an informative alternative. Tuber et al. [7] visualized water in the cathode channels of a PEM fuel

* Corresponding author. Tel.: +1 650 723 2632; fax: +1 650 723 7657.
E-mail address: julie.steinbrenner@stanford.edu (J.E. Steinbrenner).

1359-4311/$ - see front matter © 2006 Elsevier Ltd. All rights reserved.
doi:10.1016/j.applthermaleng.2006.07.020

Nomenclature

P	wetted perimeter (m)	C	geometric factor for friction factor
A	cross-sectional area (m)	Ψ	correction factor for two-fluids interaction
τ_w	wall shear stress coefficient (kg/m s^2)		
τ_i	interface shear stress coefficient (kg/m s^2)	*Subscripts*	
Re	Reynolds number	G	gas phase (air)
f	friction factor	L	liquid phase (water)
u	velocity (m/s)		
ρ	density (kg/m^3)		

cell, but did not make quantitative measurements of the film extent. There have been multiple studies examining the liquid component of two-phase flows in microchannels in terms of void fraction measurements using white light and fluorescent imaging regardless of flow regime [8–10]. Ursenbacher [11] and Wojtan [12] suggest a PLIF technique that reveals the shape of the liquid–vapor interface of stratified flow by reconstruction of distorted images.

This paper develops a fluorescence technique for measuring the liquid film thickness distribution and determining flow regimes in microchannels relevant to PEM fuel cells. Microfabricated silicon microchannels replicate those found in PEMFC gas delivery systems, while water injected into the channels simulates liquid entering the cathode channel due to chemical reaction and electro-osmotic drag. This approach allows for a controlled water "production" without the unsteady, non-uniform behavior of actual fuel cell reactions. This is of particular importance in order to decouple the problem of water entrainment into the microchannels. The water, seeded with fluorescein dye, is imaged through a microscope onto a CCD camera. Liquid film thickness is determined by counting pixels above a threshold intensity. Threshold values are determined by examining the intensity profile and uncertainties due to setting the threshold intensity are considered. Film thickness data is shown as a function of air and water flow rates and compared with the predictions of a separated two-phase flow model. Significant trends in the data which characterize the flow regime are discussed.

This data is critical for improving models for two-phase transport in PEM gas delivery microchannels. The technique developed here provides important information about the interactions between the gas and liquid phases in the microchannels, a major driving force behind heat and mass transport management within the fuel cell.

2. Experimental method

2.1. Microfabricated experimental structures

The micromachined silicon test structure is depicted in Fig. 1. Water is injected into a rectangular air channel at a single location approximately one-third of the channel length from the inlet of the gas channel. The 45 μm deep channels are carved using the process of deep reaction ion etching (DRIE). Through holes are also created using DRIE to form inlets and outlets for the fluids. Pyrex glass is anodically bonded to the silicon wafer to seal the channel and provide optical access [13]. Channel depth is controlled by the etching time. The channel depth of 45 μm was verified by focusing a calibrated microscope on the top and bottom channel surfaces.

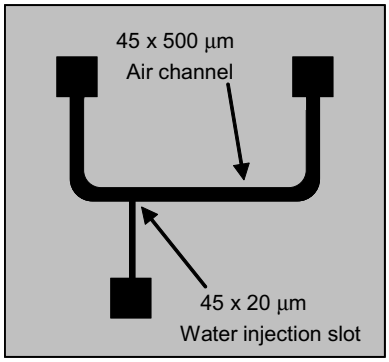

Fig. 1. Diagram of a microfabricated silicon experimental structure. A 2.37 cm U-shaped air channel with rectangular cross-section (500 × 45 μm) simulates the cathode gas delivery channels of a fuel cell. Water is injected through a 45 × 20 μm slot.

2.2. Experimental apparatus

Fig. 2 shows the setup for controlling experimental parameters. The experimental structure is placed faced down upon an inverted microscope. Images of the flow are captured with a CCD camera (1392 × 1040 pixels). A 10× objective lens allows the full 500 μm width of the channel to be captured in a single image, with each square pixel corresponding to a 0.465 by 0.465 μm area.

A differential pressure transducer in-line parallel with the chip measures the pressure drop across the microchannel. Compressibility calculations verify that the error introduced by the contraction of the flow path from 1/8 in. OD teflon tubing to the rectangular channel is negligible. The air flow rate is varied by adjusting a downstream needle valve under choked flow exit conditions. Tubing lengths

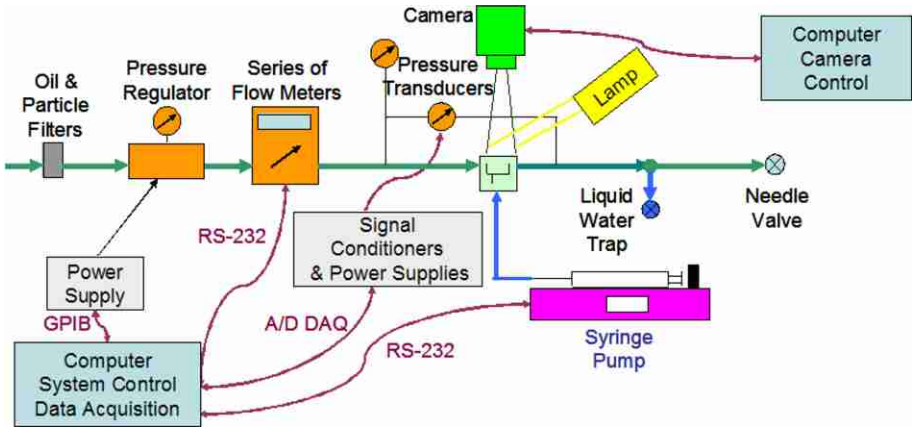

Fig. 2. Schematic of experimental setup.

downstream are minimized to reduce settling time between exit pressure conditions when the needle valve is adjusted.

2.3. Fluorescent imaging

Fluorescent imaging provides detailed information about the flow regime and water film extent within the channel. Using fluorescence imaging, the air/water interfaces are more clearly distinguishable than with white light imaging. Fig. 3 is a comparison of white light and fluorescence imaging of the injection region for a single stratified flow within the microchannel. Water injected into the channels is seeded with a 0.5 mmol concentration of fluorescein dye to enable fluorescent visualization of the flow. Fluorescence excitation is achieved with a broadband metal halide lamp combined with an FITC filter cube on an inverted microscope.

2.4. Measurement procedure

Fluorescent images are captured at multiple water flow rates for fixed inlet air pressures and varying exit pressures. For an inlet pressure of 15 psig, average inlet air velocities ranging from less than 1 m/s to greater than 25 m/s were achieved. For an inlet pressure of 30 psig, maximum air velocities approaching 60 m/s are attained. At each exit pressure, images of the flow are captured once the system achieves a steady state. Between settings, the channel is evacuated of water by opening the exit valve to atmospheric and allowing the air to clear the water film. This prevents any surface tension induced hysteresis.

Under most flow conditions, fluorescent images are taken at a single location approximately halfway between the water injection slot and the downstream bend of the channel. At low air velocities, large fluctuations in the film thickness along the length of the channel were observed and therefore multiple locations along the length of the channel are imaged. Under high air flow rates, a downstream instability develops in the film, causing the appearance of wisps of fluid departing from the film into the air stream. In these cases, the film thickness is measured closer to the water injection point where a stable film adheres to the wall.

Absolute and differential pressure and mass flow rate measurements are also recorded at each flow condition. Pressure measurements were collected and averaged in sets of 100 readings. Mass flow rates were measured at 12.5 Hz and averaged over at least 30 s.

2.5. Data analysis

Average inlet air velocity values are calculated from the measured mass flow rates. The mass flow rate is divided by

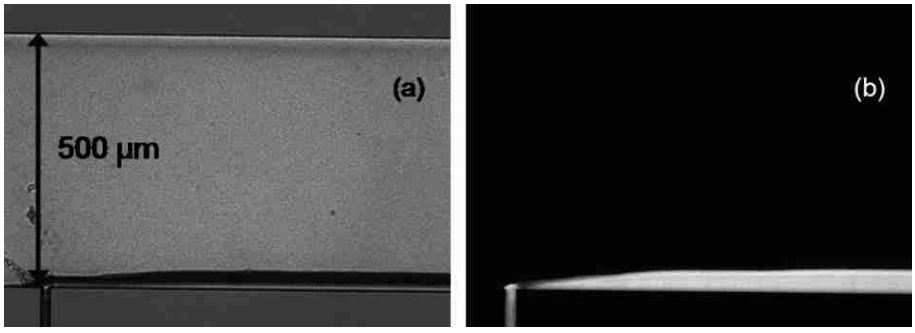

Fig. 3. Comparison of (a) white light and (b) fluorescent imaging of water injection region of stratified air–water flow in 500×45 μm channel. Water injection slot measures 20×45 μm, creating a nearly two-dimensional flow.

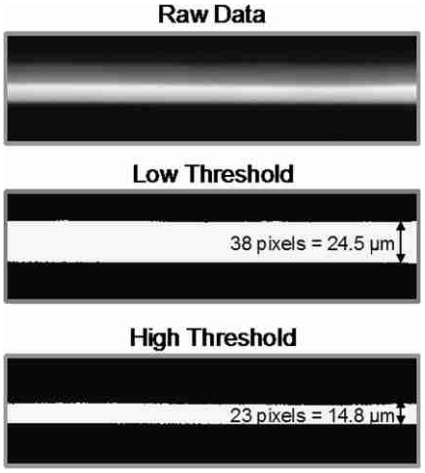

Fig. 4. Thresholding technique. Large difference in film thickness between high and low threshold measurements only appears in high air velocity, low water flow rate conditions. It may indicate the presence of interface curvature in the 3rd dimension. (Air velocity = 22.9 m/s, Water injection rate = 10 μl/min).

the temperature and pressure dependent air density and the cross-sectional area of the gas channel.

Film thickness measurements are extracted from fluorescent images of the flow using a simple threshold intensity pixel counting technique. After subtracting the average background intensity from each image, the profile of the intensity was examined at a typical flow cross-section. From this profile, two threshold values of intensity were determined, representing a low and a high intensity reading which might reasonably represent the edge of the film. Typical background intensity was 100; typical film intensity was 900. The threshold values were set at intensities of 250 and 600. Upon examination of many of the images, it was determined that the same threshold values were valid for all images.

For each threshold value, images are processed such that each pixel with intensity greater than the threshold is assigned a binary value of 1, otherwise the pixel is assigned a value of 0. Fig. 4 illustrates the transformation of a raw image into high and low threshold binary images. In this manner, the film thickness at each cross-section of the channel is easily calculated by summing a column of pixels. There are 1392 cross-sections (columns) in each image, and the recorded film thickness is the average over these cross-sections. For conditions at which the flow exhibits large stationary waves, the film thickness is averaged over all of the images collected.

2.6. Uncertainty

2.6.1. Velocity

Two mass flow meter readings were compared: a thermal mass flow meter with a quoted accuracy of ±3% measured value, and a laminar pressure drop flow meter with an accuracy of ±0.015 SLPM. Velocities calculated from the thermal mass flow meter readings are reported with an accuracy of ±5% MV, including uncertainties in the channel depth and air density. There is a constant velocity offset of 1.2 m/s between the two flow meter readings.

2.6.2. Film thickness

There are several sources of uncertainty in this optical measurement technique. Less significant sources include the two-dimensional nature of the measurement which yields depth-averaged fluorescence intensities that are a function of the depth of field of the microscope objective as well as limitations of resolution due to finite pixel dimensions. In some cases, optical effects cause unphysical variations in fluorescent intensity near the edge of the film likely due to internal reflection by incident, scattered, and emitted light. These fluctuations may be an obstacle when extracting quantitative information from fluorescent intensity, but they do not significantly affect this thresholding technique.

Uncertainty due to threshold value setting for the film becomes significant at high air flow rate, low water flow rate cases as shown in Fig. 4. Under these conditions there is a grey region of nearly 10 μm between the film thickness measured by high and low threshold values. This interesting phenomenon may be due to the presence of a meniscus or three-dimensional shape of the fluid film, which causes regions of lower fluorescent intensity at the top and bottom of the channel and blurs the appearance of the interface in the two-dimensional imaging technique, which is focused near the vertical center of the channel. Other means of capturing this flow phenomenon and reducing this uncertainty are being investigated. The results presented in this paper use the average of the thicknesses calculated from the two threshold values. The error bars for this uncertainty are shown at high air velocities.

Alternatively error bars on low air velocity, large film thicknesses represent the conditions of high water flow rate and low air flow rates which create stationery waves in the film along the length of the channel. The magnitude of these waves varies with flow conditions. Of the images recorded along the length of the channel, the standard deviation of film thickness due to variation in film thickness was around 50 μm. A transition occurs when the film thickness is less than about 100 μm, and these stationary waves are no longer observed. An appropriate explanation and non-dimensional parameter for this transition is being pursued.

3. Stratified two-phase model

A one-dimensional separated two-phase flow model has been developed to predict the liquid film thickness in a rectangular channel with a flat air–water interface as sketched in Fig. 5. Considering each fluid separately and neglecting mass exchange between the two-phases, the model solves mass and momentum conservation equations in the flow direction assuming equal pressure gradients for each fluid,

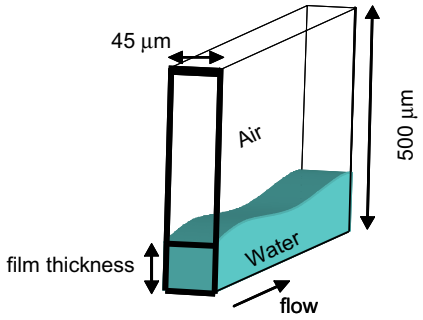

Fig. 5. Cross-sectional plane for two-dimensional stratified two-phase flow model. Film thickness is calculated by equating air and water pressure gradients in the flow direction, with equal interface shear stress and velocities.

$$\tau_{wG}\frac{P_G}{A_G}-\tau_{wL}\frac{P_L}{A_L}+\tau_i P_i\left(\frac{1}{A_G}+\frac{1}{A_L}\right)=0 \quad (1)$$

where P and A are the wetted perimeters and cross-sectional areas, respectively. Both depend on the film thickness. τ_{wL} and τ_{wG} represent the wall shear stress in the liquid and gas phase respectively, while τ_i represents the shear at the interface between the two fluids. The shear stresses account for both the channel geometry and the interaction of the two-phases (moving interface) by means of a modified friction factor,

$$\tau=\frac{1}{2}\rho u^2 f, \quad \text{where } fRe=C\cdot\Psi \quad (2)$$

This friction factor multiplies a geometric component, C, based on the aspect ratio of the channel by an interface modification factor, Ψ, which is derived from an analytical solution to stratified two-phase flow between infinite plates.

4. Results and discussion

Film thickness data are plotted as a function of air flow rate for four water injection rates in Fig. 6. For a given water injection rate, the liquid film thickness decreases non-linearly as air velocity increases. When the film is thick, it is very sensitive to the air velocity. Slight increases in air velocity result in substantial decrease of the film thickness. At high air flow rates, the water film thickness asymptotes toward a minimum film thickness. Further increases in air flow rate no longer affect a substantial increase in the water velocity. Interestingly, these are the same conditions under which a gray intensity region causes uncertainty in the edge of the water film and the shape of the air–water interface. The stratified water film may transition to a new flow regime in order to adjust to the increasing air velocity.

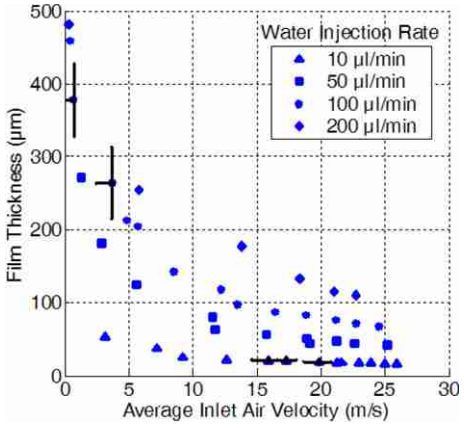

Fig. 6. Liquid film thickness data for four injection rates in a rectangular microchannel as a function of air velocity for an inlet pressure of 2 atm.

At low air flow rates, the water film fills a large portion of the channel, forming stationary waves along the length of the channel, which could be the result of varying surface tension forces along the wall balancing inertial and shear forces under low air flow. Another explanation for this shape could be the interaction of purely fluidic forces in the channel, although this seems unlikely due to the large relative magnitude of surface forces in the channel. Higher air flow rates suppress the growth of the liquid film and the stationary waves dissolve into a flat film as the water velocity increases. This transition occurs around a film thickness of 100 μm.

Higher water injection rates increase the film thickness and decrease the air flow rate for a given pressure drop across the chip. This effect is most prominent when water injection rates are low and changes in injection rate produce larger increases in film thickness.

Fig. 7 examines two of the above cases in detail and compares measured film thickness data with those predicted by the two-phase stratified flow model described in

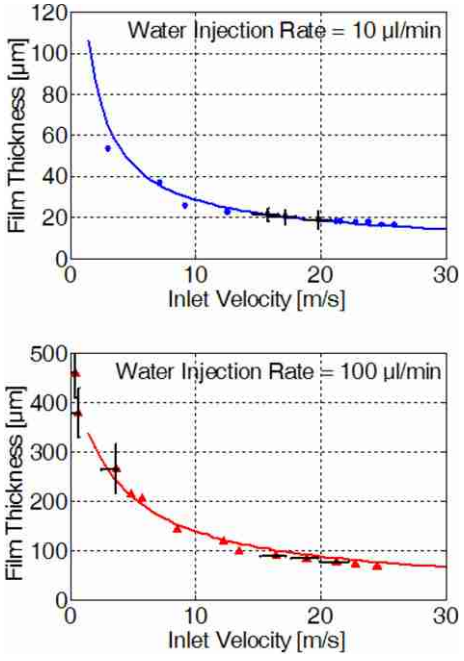

Fig. 7. Liquid film thickness data compared to predictions of a stratified two-phase flow model for two water injection rates in a 500×45 μm rectangular microchannel ($C=21.4$, $\Psi_L\gg0.5$, $\Psi_G\gg1$, $\Psi_i\gg1$).

the previous section. The model accurately predicts the measured film thickness for the geometry and flow rates considered, both at a low water injection rate and at a high water injection rate, as depicted in Fig. 7.

5. Summary and conclusions

The measurement scheme presented in this paper is an important tool for understanding, observing, and measuring flow regimes and flow regime transitions in two-phase microchannel flow. We have measured liquid film extent in stratified two-phase microchannel flows for the purpose of characterizing flow regime parameters and transitions. This information is used to verify model predictions of the two-phase flow, providing insight into the flow physics. Future experiments will incorporate heating and humidification of the channels to examine heat and mass transfer phenomena in stratified and other two-phase flow regimes in microchannels.

Acknowledgements

The authors would like to thank our sponsor, Honda R&D Co. Ltd., not only for their support but also for their input, feedback and insight into the project, as well as the Stanford Graduate Fellowship Program for the financial support of Julie Steinbrenner.

References

[1] S.W. Cha, R. O'Hayre, S.J. Lee, Y. Saito, F.B. Prinz, Geometric scale effect of flow channels on performance of fuel cells, J. Electrochem. Soc. 151 (11) (2004) A1856–A1864.

[2] G.G. Park, Y.J. Sohn, S.D. Yim, T.H. Yang, Y.G. Yoon, W.Y. Lee, C.S. Kim, Influence of water behavior in the gas diffusion layer on the performance of PEMFC, Fuel Cell Science Engineering and Technology, Rochester, NY, 2004, 14–16 June.

[3] N.P. Siegel, M.W. Ellis, D.J. Nelson, M.R. von Spakovsky, A two-dimensional computational model of a PEMFC with liquid water transport, J. Power Sources 128 (2) (2004) 173–184.

[4] U. Pasaogullari, C.Y. Wang, Liquid water transport in gas diffusion layer of polymer electrolyte fuel cells, J. Electrochem. Soc. 151 (3) (2004) A399–A406.

[5] P. Stahl, P.R. von Rohr, On the accuracy of void fraction measurements by single-beam gamma-densitometry for gas–liquid two-phase flows in pipes, Exp. Therm. Fluid Sci. 28 (6) (2004) 533–544.

[6] C.W. Snoek, Selection of new developments in multiphase flow measurement techniques, Exp. Therm. Fluid Sci. 3 (1) (1990) 60–73.

[7] K. Tuber, D. Pocza, C. Hebling, Visualization of water buildup in the cathode of a transparent PEM fuel cell, J. Power Sources 124 (2) (2003) 403–414.

[8] M. Kawaji, A. Kawahara, P.M.Y. Chung, M. Sadatomi, K. Okayama, Effects of channel diameter and liquid property on void fraction in adiabatic two-phase flow through microchannels, in: Second International Conference on Microchannels and Minichannels, 17–19 June 2004, Rochester, NY, pp. 381–388.

[9] S. Angelini, W.M. Quam, W.W. Yuen, T.G. Theofanous, FLUTE: fluorescent technique for two-phase flow liquid-fraction measurements, Chem. Eng. Commun. 118 (1992) 237–249.

[10] D. Fogg, R. Flynn, C. Hidrovo, L. Zhang, K. Goodson, Fluorescent imaging of void fraction in two-phase microchannels, in: 3rd Int. Symposium on Two-phase Flow Modeling and Experimentation, 22–24 September 2004, Pisa, Italy.

[11] T. Ursenbacher, L. Wojtan, J.R. Thome, Interfacial measurement in stratified types of flow. Part I: New optical measurement technique and dry angle measurements, Int. J. Multiphase Flow 30 (2) (2004) 107–124.

[12] L. Wojtan, T. Ursenbacher, J.R. Thome, Interfacial measurement in stratified types of flow. Part II: Measurements for R-22 and R-410A, Int. J. Multiphase Flow 30 (2) (2004) 125–137.

[13] F.M. Wang, J.E. Steinbrenner, C.H. Hidrovo, T.A. Kramer, E.S. Lee, S. Vigneron, J.K. Eaton, K.E. Goodson, Microfabricated experimental structures for the investigation of two-phase transport phenomena in microchannels, Heat SET 2005: Heat Transfer in Components and Systems for Sustainable Energy Technologies, 5–7 April 2005, Grenoble, France, Appl. Therm. Eng., in press.